SUPPLEMENTARY INFORMATION

Novel Ricin Subunit Antigens with Enhanced Capacity to Elicit Toxin-Neutralizing Antibody Responses in Mice

Newton Wahome[1,#], Erin Sully[2,#], Christopher Singer[4,#], Justin C. Thomas[1,a], Lei Hu[1,b], Sangeeta B. Joshi[1], David B. Volkin[1], Jianwen Fang[5,c], John Karanicolas[6], Donald J. Jacobs[4], Nicholas J. Mantis[2,3], C. Russell Middaugh[1]*

From the [1]Macromolecule and Vaccine Stabilization Center,
Department of Pharmaceutical Chemistry, University of Kansas, Lawrence, KS 66047

[2]Division of Infectious Disease, Wadsworth Center,
New York State Department of Health, Albany, NY 12208

[3]Department of Biomedical Sciences,
University at Albany School of Public Health, Albany, NY 12201

[4]Department of Physics and Optical Science,
University of North Carolina at Charlotte, Charlotte, NC 28223

[5]Applied Bioinformatics Laboratory, University of Kansas, Lawrence, KS 66047

[6]Center for Computational Biology and Department of Molecular Biosciences,
University of Kansas, Lawrence, KS 66045

*To whom correspondence should be addressed: C. Russell Middaugh, Macromolecule and Vaccine Stabilization Center, Department of Pharmaceutical Chemistry, 2030 Becker Drive, Lawrence, KS 66047. telephone: (785) 864-5813; fax: (785) 864-5736; e-mail: middaugh@ku.edu

Donald J. Jacobs, Department of Physics and Optical Science, University of North Carolina at Charlotte, Charlotte, NC 28223. telephone: (704) 687-8143; fax: (704) 687-3160 email: djacobs1@uncc.edu

and Nicholas J. Mantis, Division of Infectious Disease, Wadsworth Center, 120 New Scotland Avenue, Albany, NY 12208. telephone: (518) 473-7487; fax: (518) 402 4773;
email: nicholas.mantis@health.ny.gov

SUPPLEMENTARY INFORMATION

Design of RiVax derivatives

The mutations in this paper were based on a previous study for enhancing RiVax thermostability through point mutations [1], that used two approaches; the RosettaDesign Suite [2,3] and the Molecular Operating Environment (MOE software suite, V. 2009.10, Chemical Computing Group). With Rosetta, new mutations were designed to improve packing in the protein core [4], yielding several mutations: V81I, C171L, and V204I (Figure S1A). The second method to enhance thermostability [5,6], identified mutations V18P, C171V and S228K (Figure S1B). The most stable of these mutations were combined as double or triple mutant substitutions.

Biophysical characterization of RiVax derivatives

Circular dichroism and tryptophan fluorescence analysis indicated that RC displayed comparable secondary and tertiary structures as compared to RiVax or RB (Fig. S2).

Immunogenicity of RiVax derivatives

Examination of serum antibody titers seven days after the first boost revealed that all four RiVax derivatives, RA, RB, SA, and SB elicited higher ricin-specific serum antibody titers than did RiVax (Fig. S3A). However, the differences in TNA were not simply due to increased antigenicity, because mice immunized with RiVax, RB and RC had only slight differences in ricin-specific IgG antibody endpoint titers (Figure S4).

Quantitative stability/flexibility relationships of RiVax mutants

The best fits to the DSC traces (Figure S5A) establish a set of empirical mDCM parameters for RiVax and each mutant protein. With the rationale that the point mutations will not substantially modify the empirical parameters from those found for RiVax, the fitting procedure is scrutinized to yield the most consistent set of empirical parameters possible (sacrificing obtaining lower fitting errors by using additional free parameters). To this end, previously established protocols are followed [7] where the conformational entropy parameter is fixed for proteins with differing sequences, but have similar structure. Therefore, in this work, 13 free parameters are independently optimized to fit all six different heat capacity curves (Table S1). In contrast, if the six proteins were unrelated, three free parameters would be required to fit to the heat capacity per protein, nominally totaling to 18 free parameters. In summary, small variations in the empirical mean-field energy parameters associated with H-bonding to solvent and atomic packing describe the heat capacity curves very well for RiVax and its five mutants (Figure S5A).

Evaluated at the temperature corresponding to the peak in heat capacity, denoted here as T_{peak}, the corresponding free energy landscape as a function of global flexibility order parameter shows typical two-state behavior for RiVax and for all but the SA mutant (Figure S5B). The SA mutant has the most distinct

DSC trace, possessing the lowest peak height and the lowest T_{peak} among all cases. The free energy curve for SA does exhibit two-state behavior, but there is a significant increase in global flexibility within the native state. While such a large shift in the native basin along the flexibility order parameter is atypically large for the majority of globular proteins studied using the mDCM, it is not unprecedented [8]. This result suggests the SA mutant may exhibit distinct functional characteristics that can be delineated.

Among all mDCM predictions, T_{peak} is the most sensitive quantity to the empirical fitting parameters, while conditional averages of mechanical properties in the native state or transition state when evaluated at the predicted T_{peak} (not experimental T_{peak}) is insensitive to parameter variation [7]. To check parameter sensitivity on T_{peak} in this work, the best-fit parameters for a given structure are applied to each of the other 5 structures (6 structures total). Specifically, there are 6 parameter sets, and 6 structures, leading to 36 cases, of which 6 cases are optimal based on fitting to the experimental data, and 30 cases (5 non-optimal parameters per structure) serve as a check on QSFR sensitivity. For a given structure, parameter differences shift T_{peak} by less than 9% relative error on the Kelvin temperature scale (Table S1). Correlation between the u, v energy parameters (Figure S6) across the dataset shows typical behavior [9], which reflects the ability for atomic packing and cross-linking H-bonding within protein structure to compensate one another. Furthermore, this cross-parameterization procedure on each mutant structure shifts its free energy landscape (at the predicted T_{peak}) by less than 0.02 degrees of freedom per residue, which is negligible. For a given parameter set, free energy landscapes across the 6 different protein structures shift by less than 0.05 degrees of freedom per residue, indicating systematic error due to structure differences is markedly low. After tuning mDCM parameters to the entire dataset for maximum self-consistency and minimal systematic error, the putative differentiating characteristics in QSFR across Rivax and its mutants are analyzed.

From the six free energy landscapes based on best-fit parameters (Figure S5B), the rank order from largest to smallest free energy barrier height in the transition state is {RB > RC > RA > SB > RiVax > SA}, which suggests mutant RB is most kinetically stable. Mutant RC, however, has a free energy barrier height near that of RB, and is also more thermodynamically stable with a greater T_{peak} (both experimental and predicted). Thus, comparing mutant RB and RC at the *same* temperature equal to the T_{peak} of mutant RB, effectively increases the free energy barrier height of RC. The mDCM prediction that RC would be measured as the most stable protein of the six is in agreement with experiment. At the other extreme, mDCM predicts SA to be least stable, also in agreement with experiment. Henceforth, the QSFR analysis is concerned with flexibility differences between RiVax and its mutants in the native state basin, and the transition state basin defined locally around the maximum of the free energy barrier.

The backbone flexibility of RiVax and its five mutants is markedly similar in the native state (Figure S7A), with a single notable differentiating characteristic occurring at residues 176 to 180 where mutants RA, RB and RC are less rigid than RiVax, and SA and SB have the same degree of rigidity as

RiVax. In the transition state, there is more variation in backbone flexibility between RiVax and its mutants (Figure S7B). Qualitatively, an overall increase in flexibility (or equivalently a decrease in rigidity) relative to the native state occurs, where some regions along the backbone gain less flexibility than other regions. For example, at residues 49 to 55 flexibility increases by the least amount, because this region is very flexible in the native state (for RiVax and all its mutants), which limits how much more flexible it can become. Upon close inspection for establishing a ranking, mutant SA exhibits the greatest backbone flexibility in the transition state, followed by SB and RB, and then by RC and RA that are more similar to RiVax but exhibit less backbone flexibility than RiVax in some regions. Rendering backbone flexibility on protein structure for RiVax in its native state, and for RiVax and for RB and RC in their transition states provides juxtapositions (Figure 5) to view differences and similarities. Although the differences are subtle, RB has the greatest backbone flexibility in the transition state, especially in the beta-sheet region at residues 55 to 95, while RC is less flexible than RiVax in a few regions, most notably within the beta-hairpin turn at residues 225 to 245. While the differences in backbone flexibility distinguish the mutants from one another, and from RiVax, these differences are very small, which is expected because the perturbation to structure is small and because backbone flexibility is generally well conserved.

The cooperativity correlation plot (CC-plot) for RiVax in the native state and transition state (Figure S8) look visually similar to the corresponding CC-plots of the mutants. However, first and second order difference CC-plots for each mutant with respect to RiVax show a rich display of characteristic differences (Figure S9A-E) that cannot be identified from backbone flexibility comparisons. In addition, to discern significant flexible and rigid correlations between pairs of residues, the CC-plots and difference CC-plots are colorized based on the signal beyond noise ratio (SBNR) as defined in the methods section. The standard deviation, σ, characterizing the base noise level is determined to be 0.025 for the NSE and 0.030 for the TSE.

The QSFR analysis as applied to RiVax and the five mutants indicates there is a variety of ways flexibility characteristics relative to RiVax can be changed upon mutation (Figure S10) to enhance the desired functional role, but these changes are often not associated with an increase in rigidity within the protein. Finally, though small systematic errors in the mDCM calculation might be introduced by the irreversibility of the thermal unfolding curves of globular proteins such as the RTA derivatives, the method adequately describes the overall thermodynamic and flexibility/rigidity trends of the varying mutants.

SUPPLEMENTARY INFORMATION

References

1. Thomas JC, O'Hara JM, Hu L, Gao FP, Joshi SB, Volkin DB, Brey RN, Fang J, Karanicolas J, Mantis NJ, Middaugh CR 2013. Effect of single-point mutations on the stability and immunogenicity of a recombinant ricin A chain subunit vaccine antigen. Hum Vaccin Immunother 9(4):740-748.
2. Das R, Baker D 2008. Macromolecular modeling with rosetta. Annu Rev Biochem 77:363-382.
3. Leaver-Fay A, Tyka M, Lewis SM, Lange OF, Thompson J, Jacak R, Kaufman K, Renfrew PD, Smith CA, Sheffler W 2011. ROSETTA3: an object-oriented software suite for the simulation and design of macromolecules. Methods in enzymology 487:545.
4. Sheffler W, Baker D 2009. RosettaHoles: rapid assessment of protein core packing for structure prediction, refinement, design, and validation. Protein Science 18(1):229-239.
5. Li Y, Middaugh CR, Fang J 2010. A novel scoring function for discriminating hyperthermophilic and mesophilic proteins with application to predicting relative thermostability of protein mutants. BMC bioinformatics 11(1):62.
6. Li Y, Zhang J, Tai D, Russell Middaugh C, Zhang Y, Fang J 2012. Prots: A fragment based protein thermo-stability potential. Proteins: Structure, Function, and Bioinformatics 80(1):81-92.
7. Livesay DR, Jacobs DJ 2006. Conserved quantitative stability/flexibility relationships (QSFR) in an orthologous RNase H pair. PROTEINS: Structure, Function, and Bioinformatics 62(1):130-143.
8. Jacobs DJ, Livesay DR, Hules J, Tasayco ML 2006. Elucidating quantitative stability/flexibility relationships within thioredoxin and its fragments using a distance constraint model. Journal of molecular biology 358(3):882-904.
9. Li T, Verma D, Tracka M, Casas-Finet J, Livesay D, Jacobs D 2013. Thermodynamic Stability and Flexibility Characteristics of Antibody Fragment Complexes. Protein and peptide letters 21(8):752-765.

SUPPLEMENTARY INFORMATION

Figure Legends

Figure S1. A) Mutations performed on RiVax with Rosetta_Holes algorithm to improve core packing: I) Mutation of valine (right), position 81, to either leucine (middle) or isoleucine (left) II) Mutation of cysteine (right), position 171, to leucine (left) III) Mutation of valine (right), position 204, to isoleucine (left). **B) Mutations performed on RiVax with MOE algorithm to improve thermostability:** I) Mutation of valine (right), position 18, to proline (left) II) Mutation of cysteine (right), position 171, to valine (left) III) Mutation of serine (right), position 228, to lysine (left)

Figure S2. Circular dichroism and intrinsic fluorescence scans of RiVax and related mutants at 10 ºC. Molar ellipticity and intrinsic tryptophan fluorescence spectra (A-D) show that the overall secondary and tertiary structure profiles of the protein mutants are similar to RiVax, albeit with the exception of mutant the circular dichroism signal of mutant RA (Figure A).

Figure S3. Ricin-specific serum antibody titers following immunization of mice with RiVax derivatives. These figures indicate that mutants RA and RB had consistently higher ricin-specific titers when compared to RiVax. Half of the SA and SB mutant ricin-specific titers were also higher than those observed in the RiVax immunized cohort.

Figure S4. Ricin-specific serum antibody titers following immunization of mice with RiVax derivatives RB and RC. RB and RC mutants had higher ricin-specific antibody titers than RiVax, but were approximately equivalent in their pair-wise titer response.

Figure S5: (A) Experimental heat capacity curves from DSC are shown as solid lines with distinct colors assigned for RiVax and its mutants. The corresponding best-fit heat capacity curves are shown using either open or filled circles while preserving the same color identification for RiVax and its mutants as defined in the legend. Despite the simplicity of the mDCM, all the fits are very good to excellent. (B) Using the same color identification, the free energy landscape is plotted versus the global flexibility order parameter at a temperature where the heat capacity is maximum (T_{peak}). Generally, T_{peak} is different for each free energy curve. For the best-fit parameters used to generate the predicted heat capacity curves as well as the T_{peak} value for each protein to generate the free energy landscapes, see **Table S1**.

SUPPLEMENTARY INFORMATION

Figure S6: As a general property of the mDCM, it has been found across all globular proteins studied to date that multiple good fits can be obtained to the heat capacity curves due to compensation between the u and v parameters, where they are linearly correlated. As the u, v parameters change along the line of correlation moving away from the best-fit case, fitting errors gradually increase. Furthermore, a similar correlation is found among best-fit u and v parameters for different proteins of similar structure and sequences when the best-fit conformational entropy parameters are similar or when there is a fixed δnat. In all cases, the u, v parameters typically correlate with one another with a regression slope near three quarters. In this work, δnat is fixed across RiVax and all of its mutants, and the best-fit u and v parameters exhibit this typical behavior as shown.

Figure S7: The flexibility index in the native state (A) and in the transition state (B) is plotted to quantify the backbone flexibility of RiVax and its mutants. The grey horizontal line defines the zero line, shown to help guide the eye. In the native state, backbone flexibility for each mutant is markedly similar to RiVax, except at residues 176 to 180 as indicated by the yellow arrow, where mutants RA, RB and RC as a group are very similar to one another, but yet significantly more flexible than RiVax, SA and SB, which form their own similar group of three. Although more differentiating features appear in the transition state, it is clearly the case that the backbone flexibility is qualitatively very similar among RiVax and its mutants.

Figure S8: The cooperativity correlation plot (CC-plot) for RiVax in the native state (A) and in the transition state (B) evaluated at T_{peak} which gives the temperature where the predicted heat capacity is maximum. The coloring is based on the signal beyond noise ratio (SBNR) that washes out (white) all correlations of magnitude less than the noise level. Red indicates a pair of residues is flexibly correlated, such that if one residue were to wiggle, it would cause the other residue to waggle. Blue indicates a pair of residues belong to the same rigid region. Note that the CC-plots are averages over many constraint network realizations in a specified ensemble, meaning that a particular pair of residues can be mutually rigid, flexibly correlated or not correlated at all across realizations. This comparison shows that the transition state loses most of its rigidity correlation because many native-like constraints break. Note that when SBNR = 1, the signal is statistically significant as far as the typical values observed in difference CC-plots across all mutations. On this scale, all mutants would have similar corresponding CC-plots in the native state and transition state with visually the same gross properties, although differences are present in all cases.

Figure S9: A) First order difference CC-plots for RA – RiVax in the native state ensemble (I), in the transition state ensemble (II) and the second order difference CC-plot for the TSE – NSE (III). B) First order difference CC-plots for RB – RiVax in the native state ensemble (I), in the transition state ensemble

(II) and the second order difference CC-plot for the TSE – NSE (III). C) First order difference CC-plots for RC – RiVax in the native state ensemble (I), in the transition state ensemble (II) and the second order difference CC-plot for the TSE – NSE (III). D) First order difference CC-plots for SA – RiVax in the native state ensemble (I), in the transition state ensemble (II) and the second order difference CC-plot for the TSE – NSE (III). E) First order difference CC-plots for SB – RiVax in the native state ensemble (I), in the transition state ensemble (II) and the second order difference CC-plot for the TSE – NSE (III).

Figure S10: The flexibility index is shaded to represent backbone flexibility in the native state (A) and in the transition state (B). (Red, Blue) represents (flexible, rigid) regions with an excess number of (degrees of freedom, constraints) in that region. White shows a balance of degrees of freedom and constraints in isostatic regions. In the last three blocks (C,D,E), only statistically significant correlations in difference CC-plots for each mutant relative to RiVax (labeled as WT on the rows in the sequence blocks) is shown except for the first entry per block, where the difference plot is relative to RB. Backbone correlations are shown for first order differences in the native state (C) and transition state (D), and for second order differences (E). (Red, Blue) shading indicates the residues are (flexibly, rigidly) correlated, while white indicates correlations below base noise. All blocks are aligned vertically for convenience, and the coloring scale between like quantities (A,B) and (C,D,E) is the same.

Tables

Table S1: Three empirical parameters u, v and δnat obtained from best fits to DSC heat capacity curves are listed for RiVax and its mutants. The units of u and v are kcal/mol, and δnat is dimensionless. T_{peak} is the temperature at the peak of the heat capacity curve, T_{ave} is the average prediction for T_{peak} using only non-optimal parameters, $\Delta T = T_{ave} - T_{peak}$, and Tsd is the standard deviation about the average temperature. All temperatures have units of Kelvin.

Table S1. Best fits of DSC heat capacity curves for RiVax derivatives

Antigen	u	v	δnat	Tpeak	Tave	ΔT	Tsd
RiVax	-2.22	-0.56	1.625	321	330.6	9.6	6.6
RA	-2.11	-0.51	1.625	320	320.5	0.5	8.4
RB	-2.03	-0.47	1.625	322	320.0	-2.0	8.5
RC	-2.11	-0.56	1.625	325	317.5	-7.5	9.2

SUPPLEMENTARY INFORMATION

SA	-1.8	-0.25	1.625	315	324.0	9.0	7.6
SB	-1.96	-0.46	1.625	321	313.5	-7.5	9.4

Figure S1A

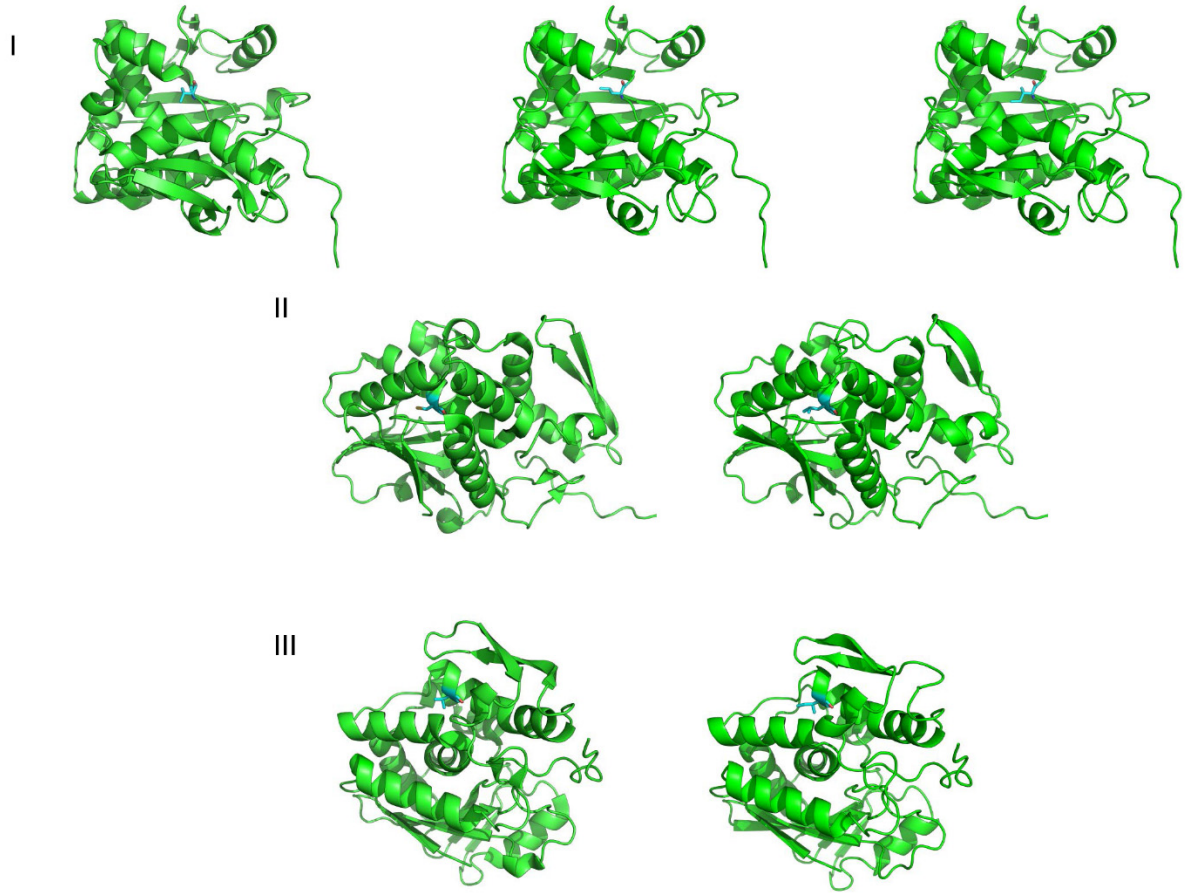

Figure S1B

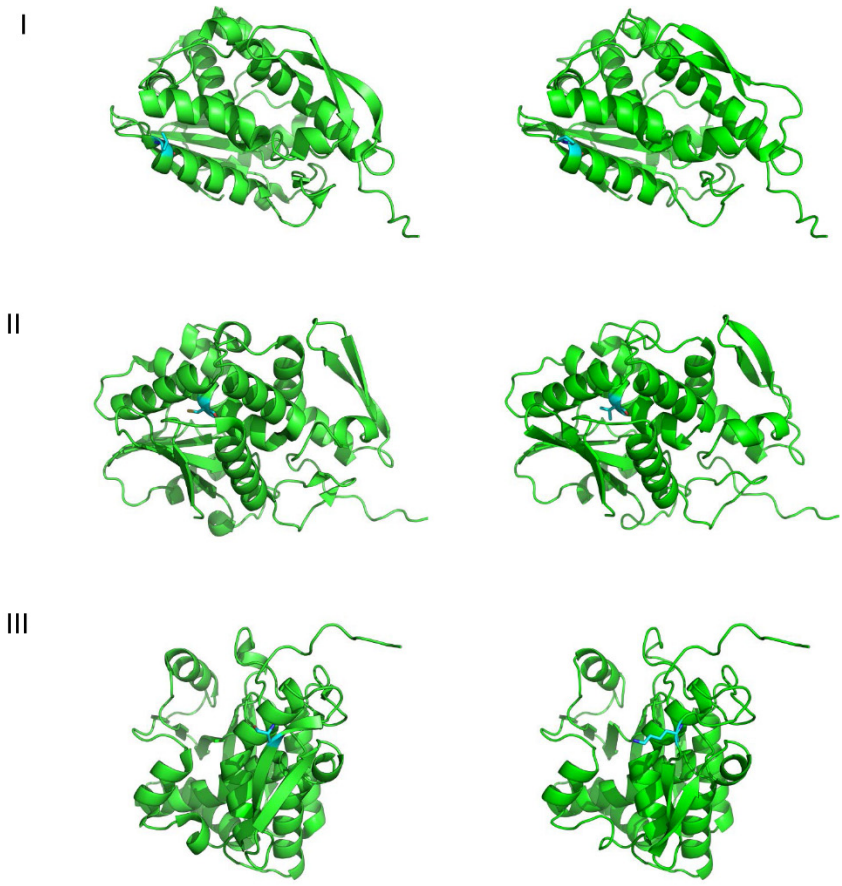

Figure S2

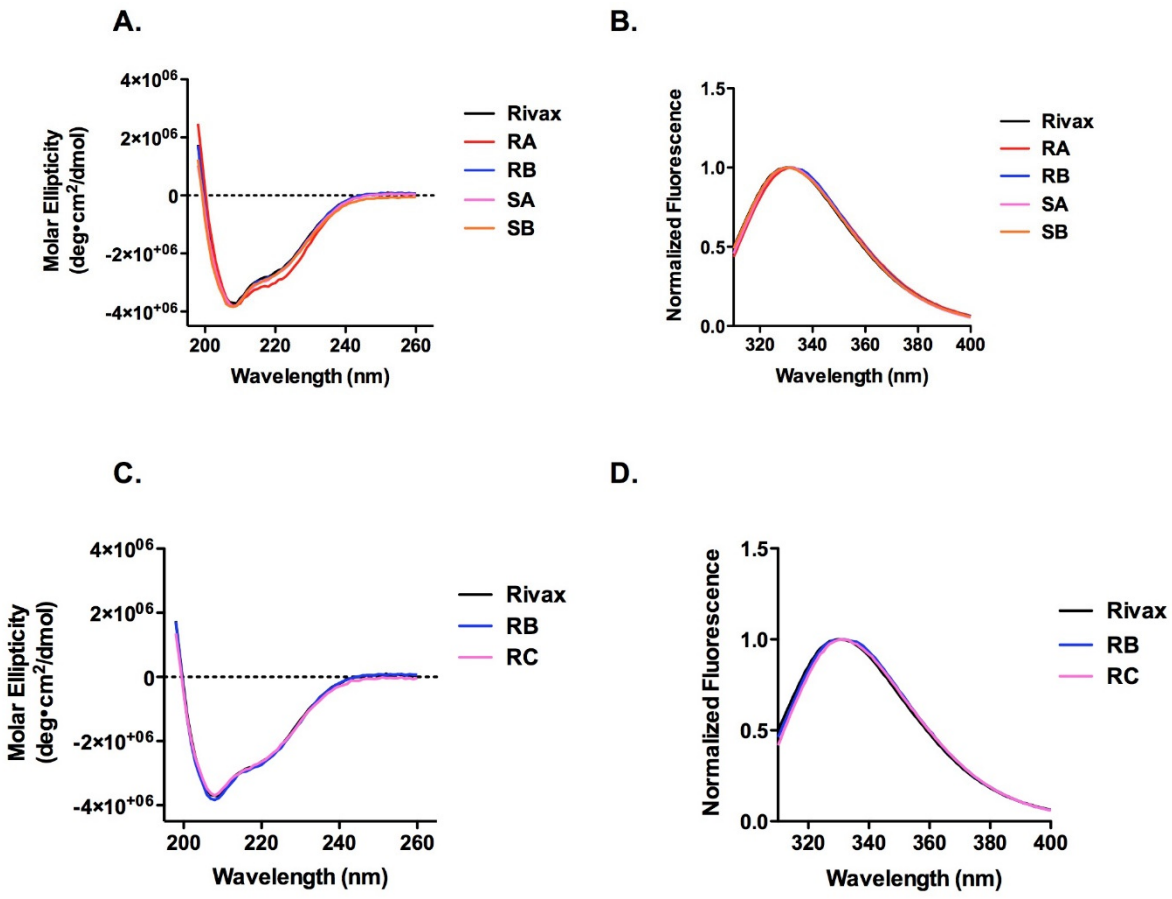
A.
Molar Ellipticity (deg•cm²/dmol)
4×10⁰⁶
2×10⁰⁶
0
-2×10⁺⁰⁶
-4×10⁺⁰⁶
200
220
240
260
Wavelength (nm)
Rivax
RA
RB
SA
SB
B.
Normalized Fluorescence
1.5
1.0
0.5
0.0
320
340
360
380
400
Wavelength (nm)
Rivax
RA
RB
SA
SB
C.
Molar Ellipticity (deg•cm²/dmol)
4×10⁰⁶
2×10⁰⁶
0
-2×10⁺⁰⁶
-4×10⁺⁰⁶
200
220
240
260
Wavelength (nm)
Rivax
RB
RC
D.
Normalized Fluorescence
1.5
1.0
0.5
0.0
320
340
360
380
400
Wavelength (nm)
Rivax
RB
RC

Figure S3

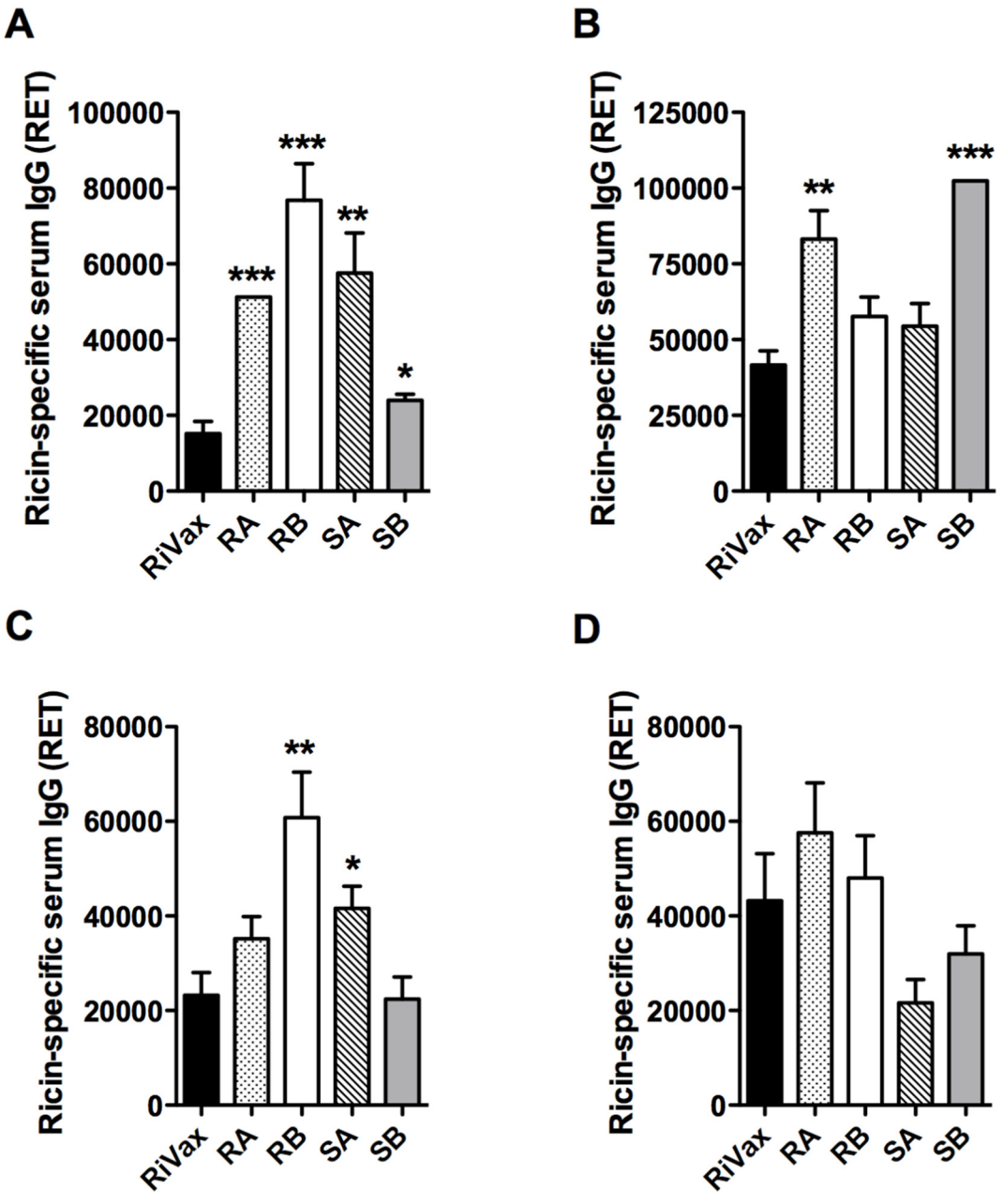
A
Ricin-specific serum IgG (RET)
100000
80000
60000
40000
20000
0
***
***
**
*
RiVax
RA
RB
SA
SB
B
Ricin-specific serum IgG (RET)
125000
100000
75000
50000
25000
0
**
***
RiVax
RA
RB
SA
SB
C
Ricin-specific serum IgG (RET)
80000
60000
40000
20000
0
**
*
RiVax
RA
RB
SA
SB
D
Ricin-specific serum IgG (RET)
80000
60000
40000
20000
0
RiVax
RA
RB
SA
SB

Figure S4

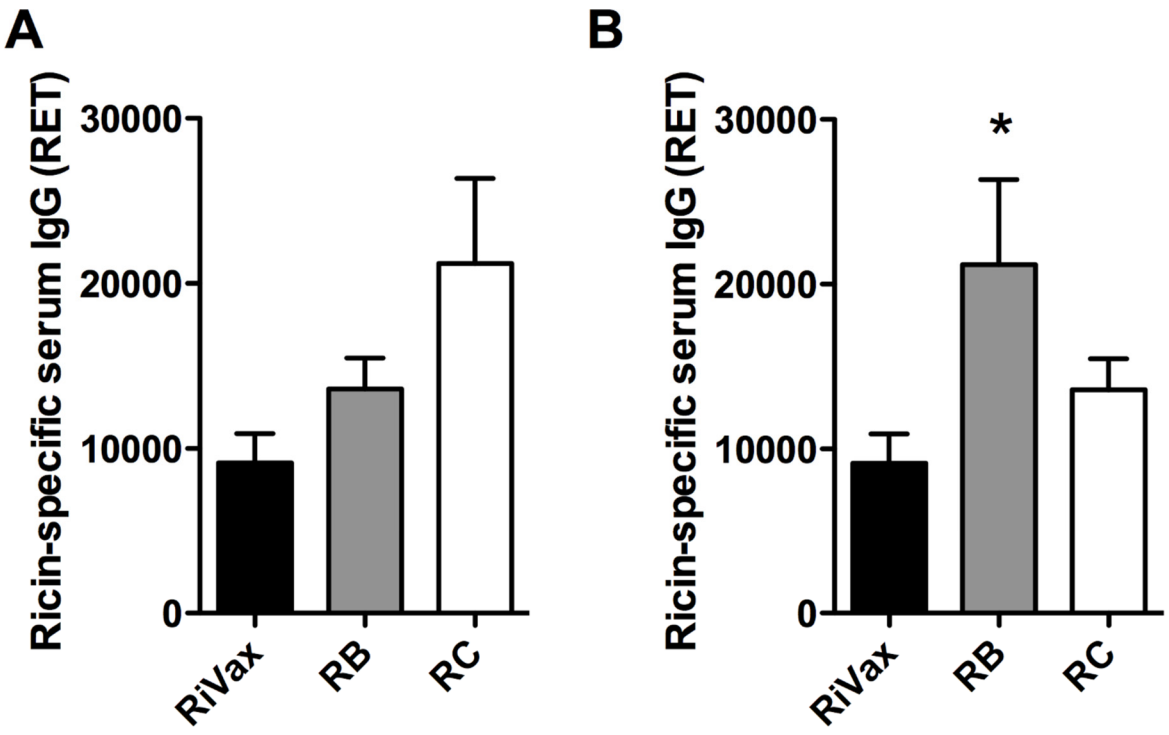
A
Ricin-specific serum IgG (RET)
30000
20000
10000
0
RiVax
RB
RC
B
Ricin-specific serum IgG (RET)
30000
20000
10000
0
*
RiVax
RB
RC

Figure S5

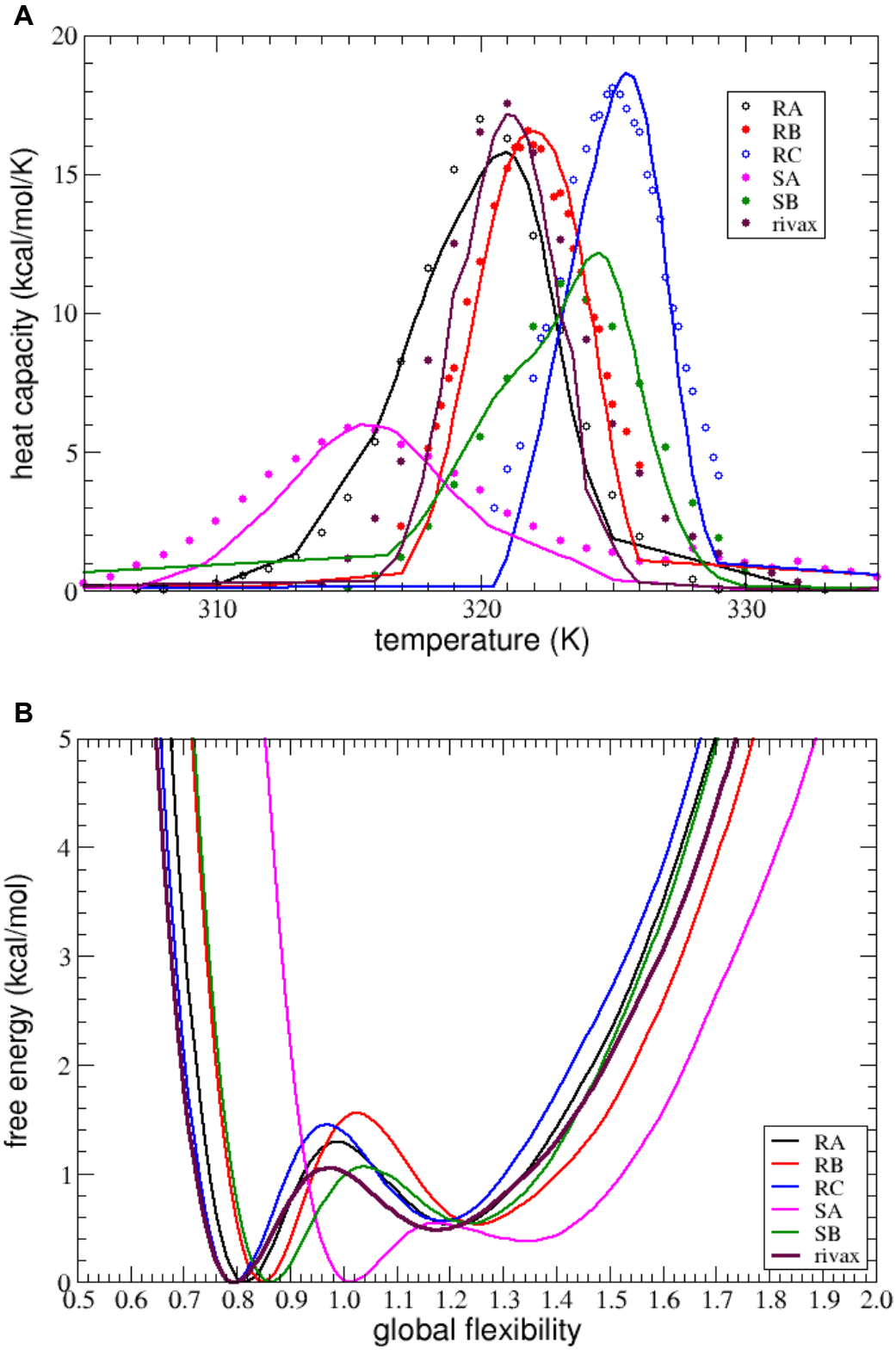
A
heat capacity (kcal/mol/K)
temperature (K)
RA
RB
RC
SA
SB
rivax
B
free energy (kcal/mol)
global flexibility
RA
RB
RC
SA
SB
rivax

Figure S6

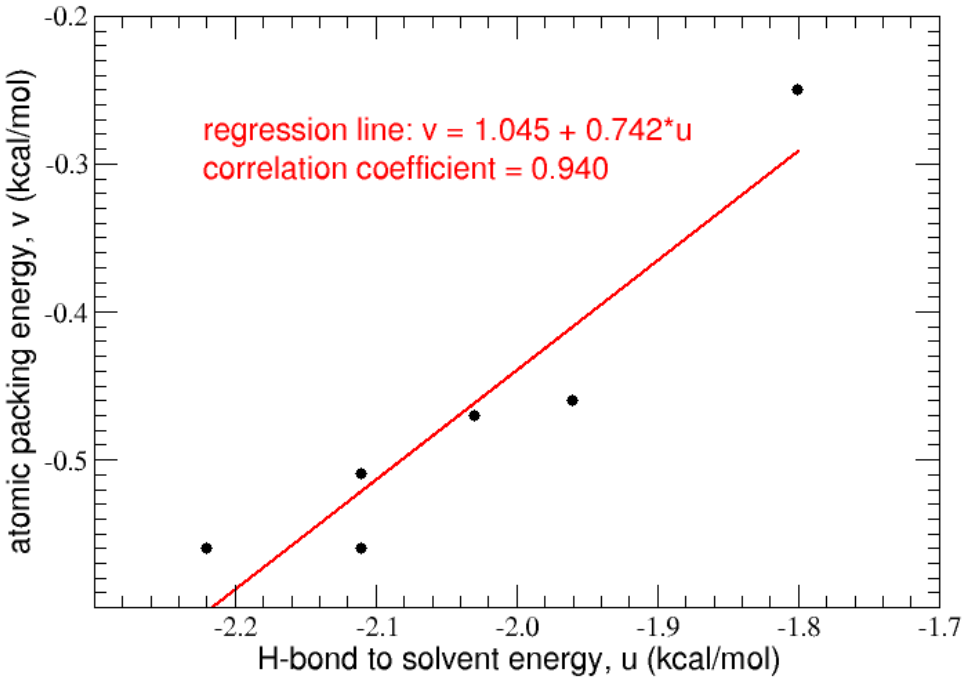
regression line: v = 1.045 + 0.742*u
correlation coefficient = 0.940
atomic packing energy, v (kcal/mol)
H-bond to solvent energy, u (kcal/mol)
-0.2
-0.3
-0.4
-0.5
-2.2
-2.1
-2.0
-1.9
-1.8
-1.7

Figure S7

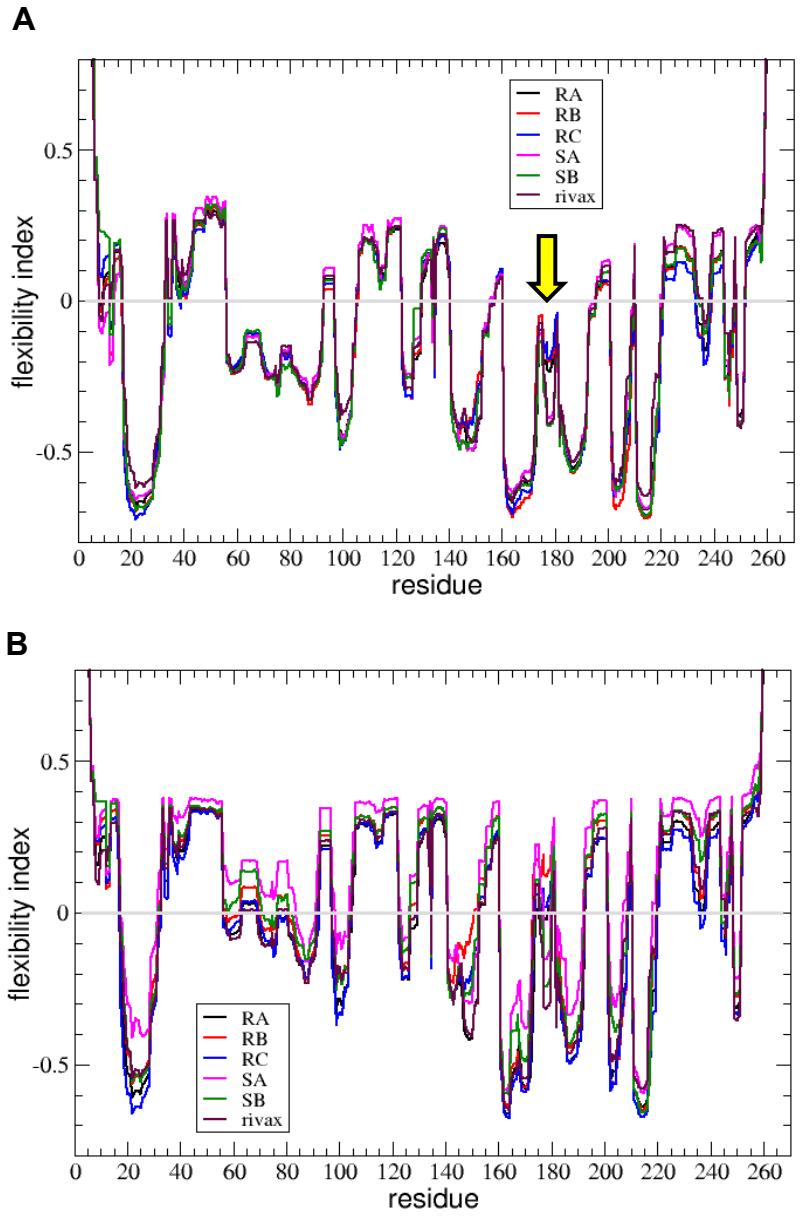
A
RA
RB
RC
SA
SB
rivax
flexibility index
0.5
0
-0.5
0 20 40 60 80 100 120 140 160 180 200 220 240 260
residue
B
RA
RB
RC
SA
SB
rivax
flexibility index
0.5
0
-0.5
0 20 40 60 80 100 120 140 160 180 200 220 240 260
residue

Figure S8

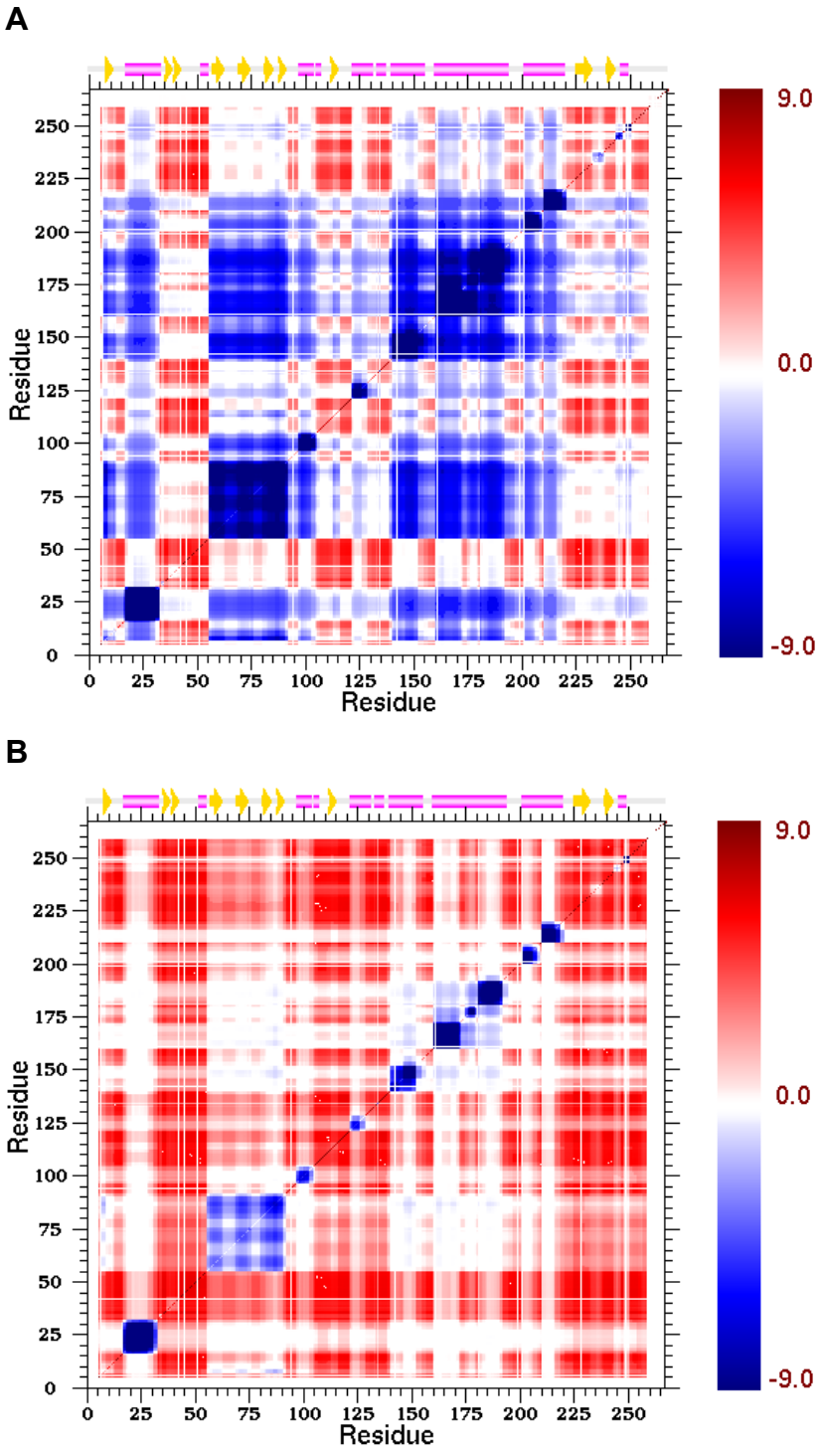
A
Residue
Residue
0
25
50
75
100
125
150
175
200
225
250
9.0
0.0
-9.0
B
Residue
Residue
0
25
50
75
100
125
150
175
200
225
250
9.0
0.0
-9.0

Figure S9A

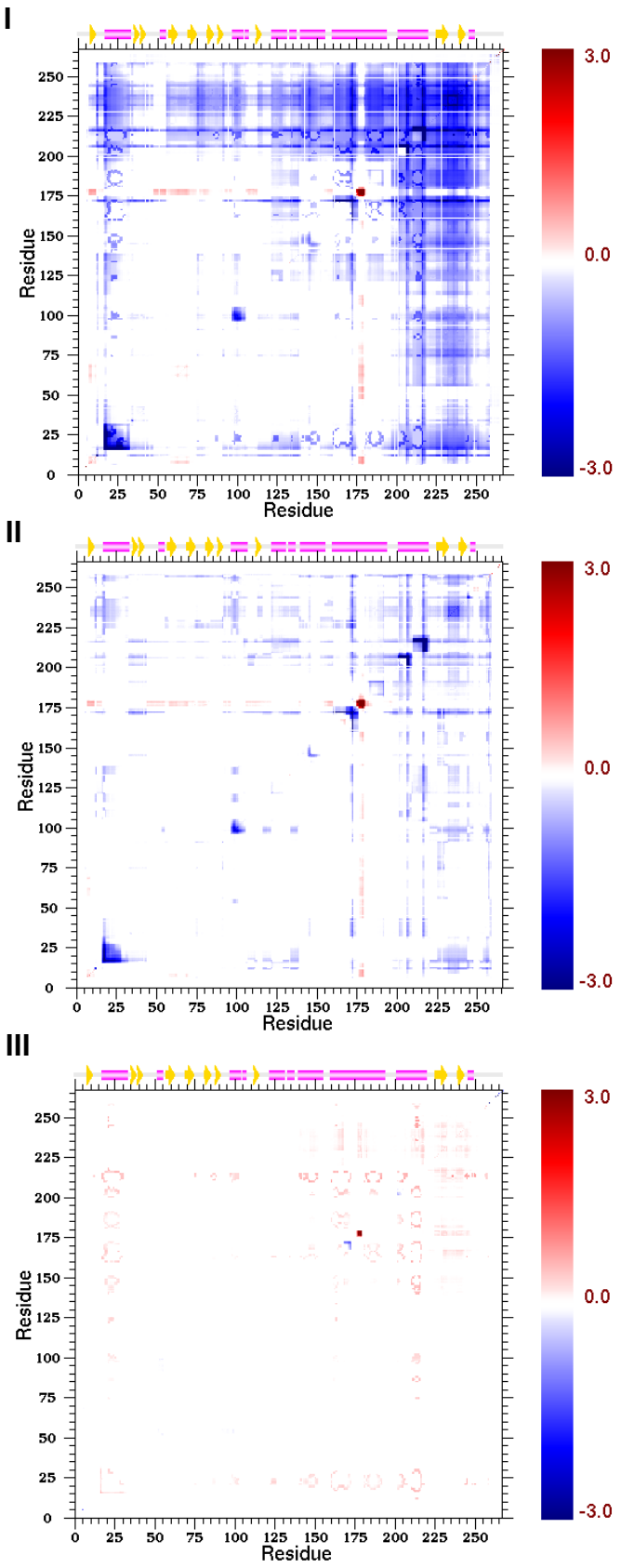
I
II
III
Residue
Residue
0
25
50
75
100
125
150
175
200
225
250
3.0
0.0
-3.0

SUPPLEMENTARY INFORMATION

Figure S9B

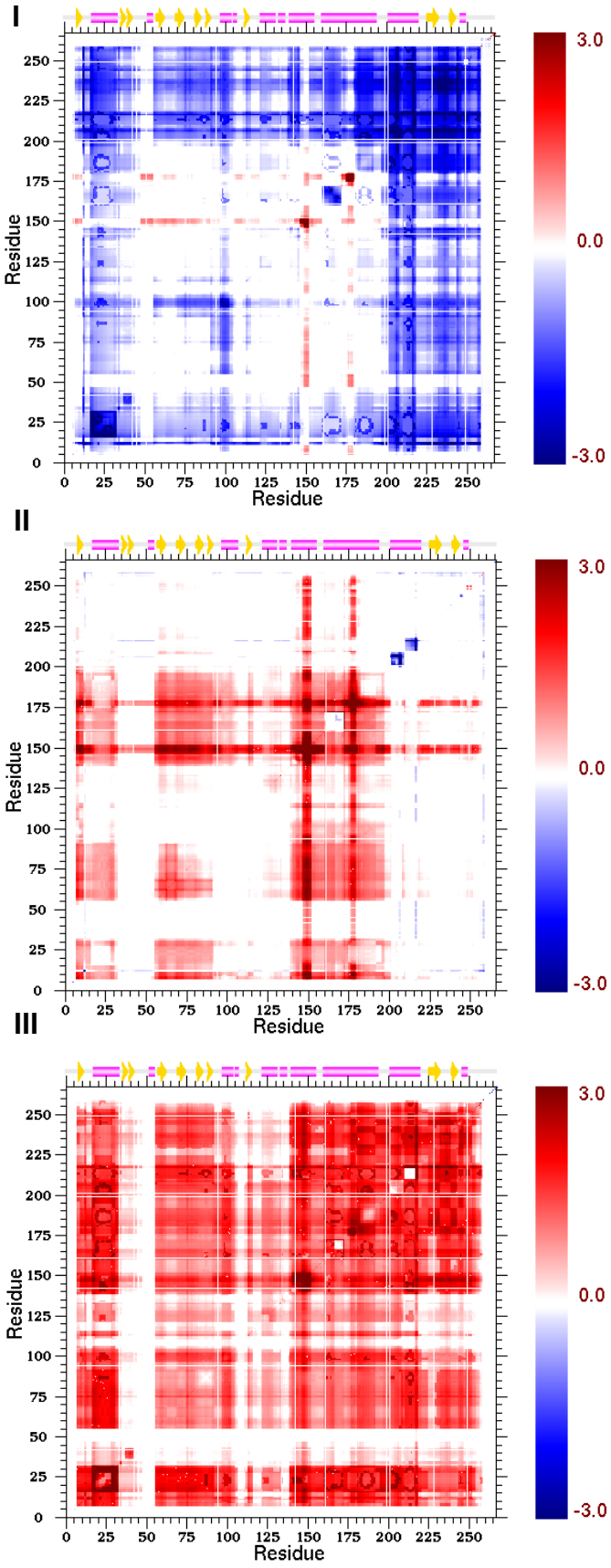

SUPPLEMENTARY INFORMATION

Figure S9C

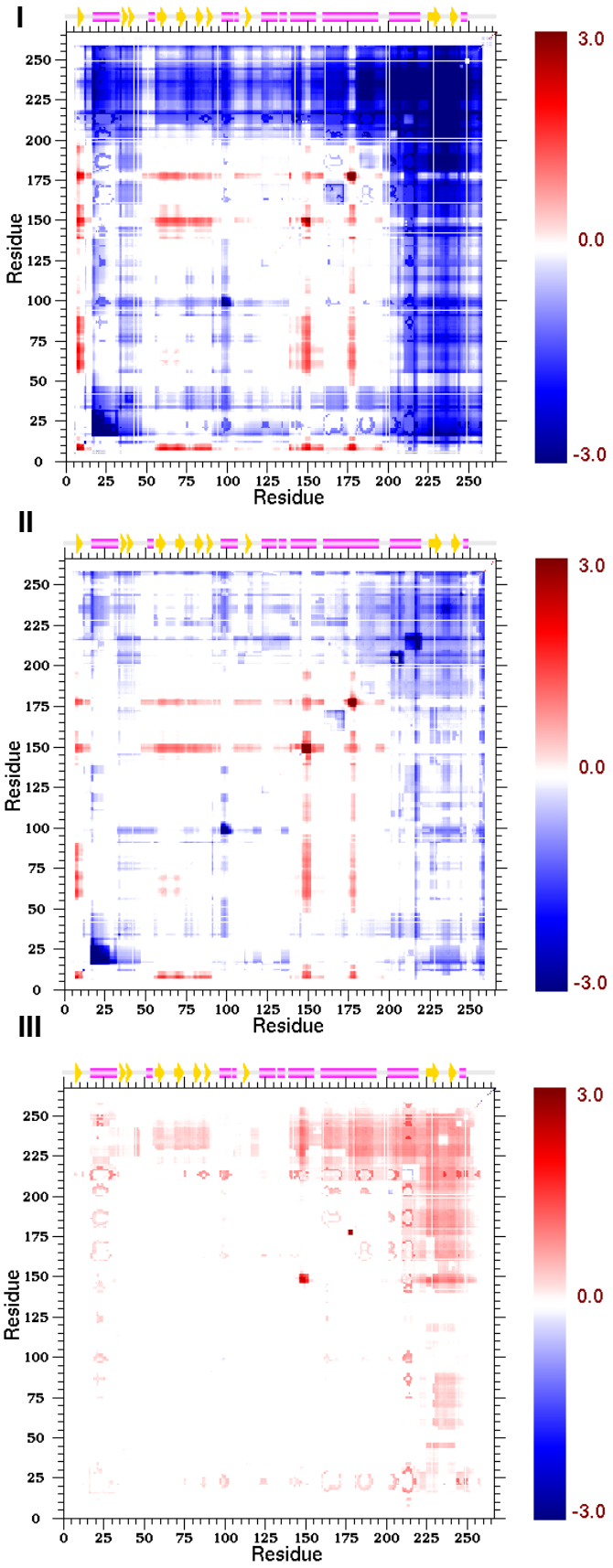

SUPPLEMENTARY INFORMATION

Figure S9D

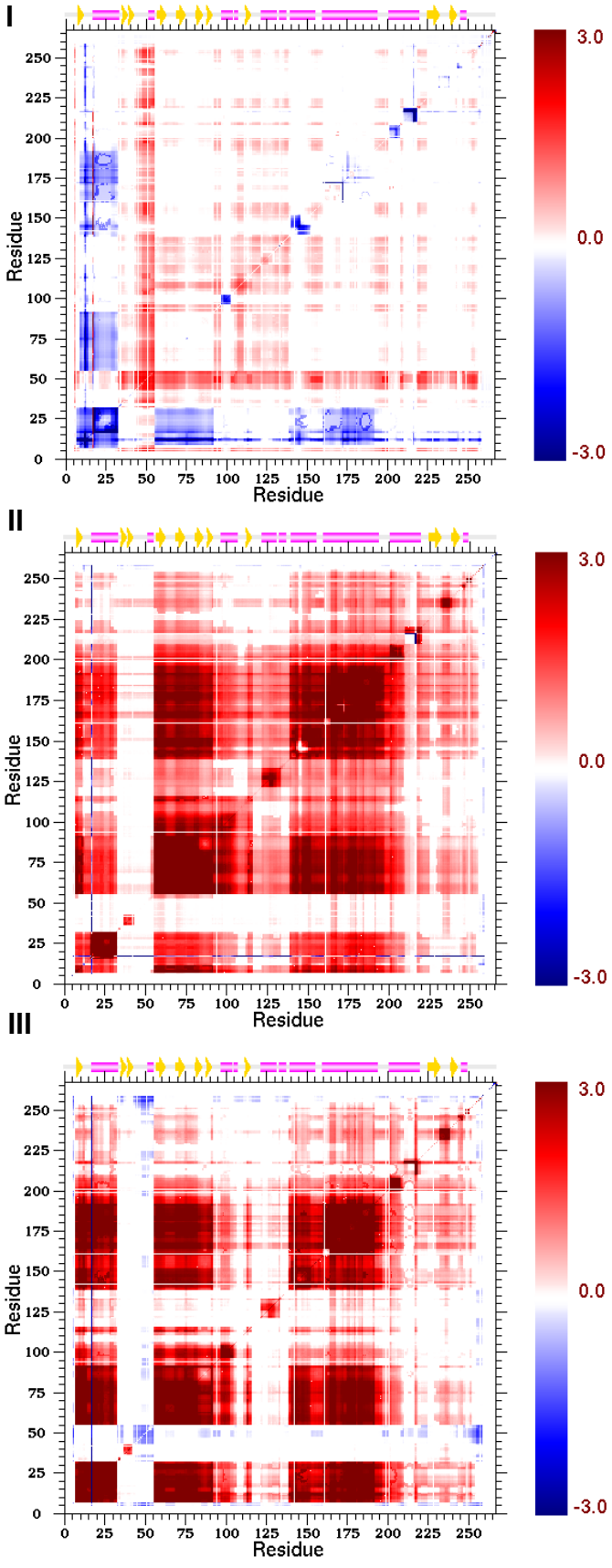

SUPPLEMENTARY INFORMATION

Figure S9E

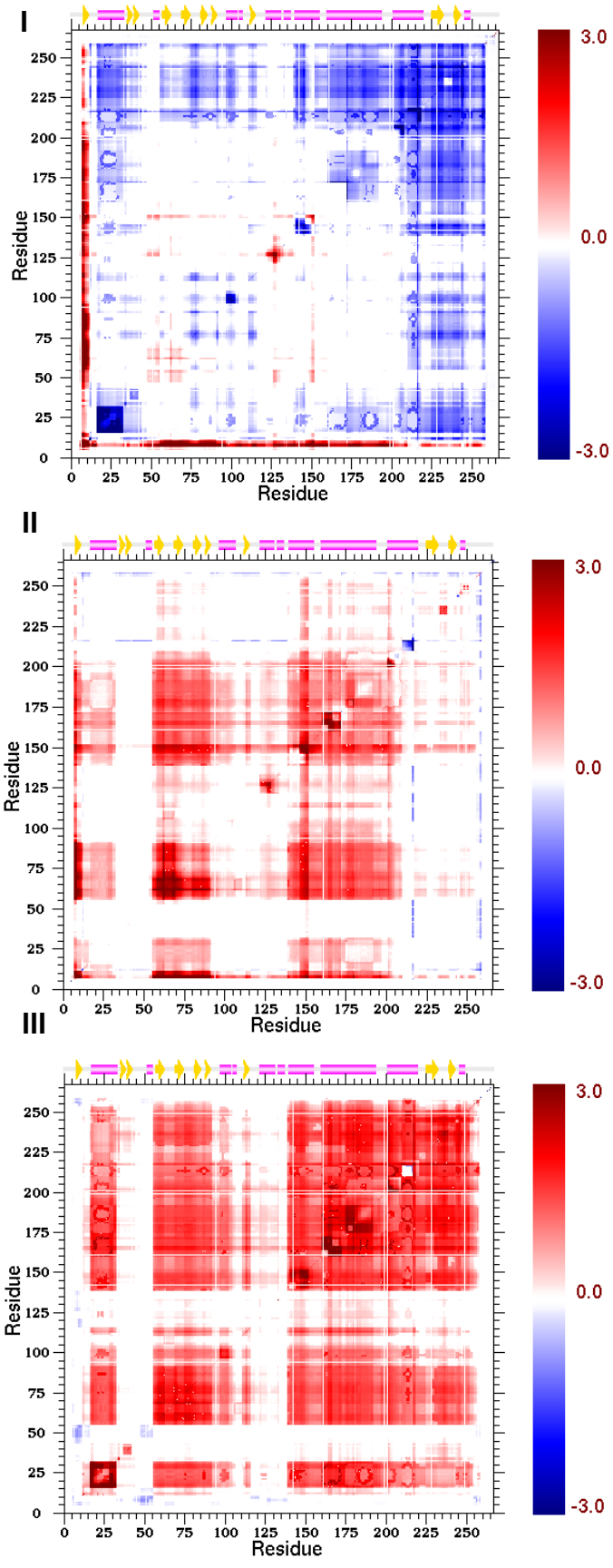

SUPPLEMENTARY INFORMATION

Figure S10